INSTITUTE OF PHYSICS PUBLISHING MODELLING AND SIMULATION IN MATERIALS SCIENCE AND ENGINEERING

Modelling Simul. Mater. Sci. Eng. **12** (2004) 1–12 PII: S0965-0393(04)80705-8

On the sweeping mechanism of dipolar dislocation loops under fatigue conditions

J Huang[1], **N M Ghoniem**[1,3] **and J Kratochvíl**[2]

[1] Mechanical and Aerospace Engineering Department, University of California, Los Angeles, CA 90095-1597, USA
[2] Faculty of Civil Engineering, Department of Physics, Czech Technical University, Thákurova 7, 16629 Prague 6, Czech Republic

E-mail: ghoniem@ucla.edu

Received 10 January 2004
Published
Online at stacks.iop.org/MSMSE/12
doi:10.1088/0965-0393/12/2/...

Abstract

Dislocation dynamics simulations of the interaction between prismatic dipolar loops and a glide screw dislocation are presented. As a result of stress gradients generated by the glide dislocation, dipolar loops execute drift motion along their glide cylinders. Simulations of the combined motion of two dipolar loops in the stress field of a glide dislocation clearly show that inter-loop forces are essential in determining their spatial trajectories. Under cyclic stress conditions, it is shown that same-type dipolar loops drift monotonically in the same direction, and that their spatial clustering is largely determined by strong inter-dipolar binding forces. The investigated sweeping mechanism is discussed in terms of the prerequisites for the formation of persistent slip bands under fatigue loading conditions.

1. Introduction

The spontaneous formation of dislocation patterns is one of the most striking features of plastic deformation of ductile crystalline solids at the micro scale. These patterns consist of alternating dislocation rich and dislocation poor regions usually in the micrometre range (e.g. dislocation bundles, veins, walls, channels, and dislocation cells). The formation of these patterns is widely believed to be a result of collective interactions between dislocations. Nonetheless, such collective phenomena play a prominent role in determining the general characteristics of plastic deformation, fatigue, and fracture properties of ductile materials.

The dislocation pattern formation process is a consequence of an overproduction of dislocations. Only a small fraction of them is needed to carry plastic deformation, while the

[3] Author to whom any correspondence should be addressed.

 © 2004 IOP Publishing Ltd Printed in the UK

Editor: BalaAnu

rest is stored in the crystal. The deformed crystal, which is supersaturated with dislocations, tends to decrease the internal energy by mutual screening of their elastic fields. If dislocations possess sufficient maneuverability provided mainly by easy cross-slip, the leading mechanism is individual screening. Dislocations are stored in the form of dipoles, which are transformed to dipolar loops of prevailing edge character (i.e. prismatic). A sweeping mechanism was proposed to explain the pattern formation [1]. Loops are swept by glide dislocations, or may drift in stress gradients to clusters, and hinder the motion of fresh glide dislocations causing strain hardening. A homogeneous distribution of loops is thus unstable. The current understanding of the above scenario is still only intuitive. The theoretical predictions [1–8] are mostly qualitative, a fully quantitative description is hindered by lack of knowledge of the specific mechanisms outlined within this framework. The main objective of the present work is to utilize the dislocation dynamics approach (e.g. [9–13]), and provide quantitative data needed for continuum and statistical models of pattering.

During the initial stages of cycling at low plastic strain amplitudes (typically $<10^{-3}$), dislocation-rich regions form a pattern known as a matrix structure consisting of snake-like veins (tangles, bundles, loop patches) oriented on average along edge dislocation directions. The veins, which are loosely organized in quasi periodic patterns are surrounded by dislocation poor channels. It has been noted that the tangle (bundles) structure observed in cubic metals at the beginning of the second stage of hardening in tension tends to form an arrangement akin in morphology and size to the vein pattern. The veins (tangles) occupy approximately 50% of the crystal volume and the density of stored dislocations in the veins increases with deformation. At a certain stage of cycling, the veins become saturated and start to be unstable. The saturation of the matrix structure is a prelude of localization of strain into thin lamellae called persistent slip bands (PSBs).

In the lamellae, the characteristic ladder structure of dipolar dislocation walls (cells) may develop gradually from leftovers of the veins. The walls and veins contain predominantly narrow prismatic loops. The basic phenomena underlying the process of plastic deformation at the micro scale is the large difference between the internal energy of an ideal crystal and a crystal with dislocations strained by the same amount. This fact creates a thermodynamic driving force which is probably the reason for the highly non-correlated generation of dislocations by the bursts of activated dislocation sources. This process results in an overproduction of dislocations. Only a small fraction of them is needed to carry plastic deformation, while the rest is stored in the crystal. Deformed crystals supersaturated with dislocations tend to decrease the internal energy by mutual screening of their elastic fields. If dislocations possess sufficient maneuverability provided namely by easy cross-slip (solids with wavy slip), the leading mechanism is individual screening. The dislocations are stored in the form of dipoles, which are transformed to dislocation dipolar loops of prevailing edge character or such loops are directly formed. The loops hinder the motion of the fresh glide dislocations causing strain hardening. A homogeneous distribution of loops is unstable. Loops are swept by glide dislocations or are drifted by stress gradients to clusters and a dislocation pattern is formed. In the clusters (tangles, veins, walls) at a sufficient concentration, loops and dislocations start to annihilate, modify the dislocation pattern, and through strain hardening control strain localization.

An approximate analytical model of sweeping of a rigid prismatic loop by a straight glide dislocation has been studied analytically [14], and a quantitative criteria for the steady sweeping of the dipolar loop is obtained. Formulae for the stress field of a prismatic rectangular loop of an infinitesimal or finite width have been derived [15, 16]. Alternatively, the components of the stress tensor generated by a single loop has been evaluated by the numerical fast sum method [17]. As these stress fields are rather complex, an accurate method is needed to

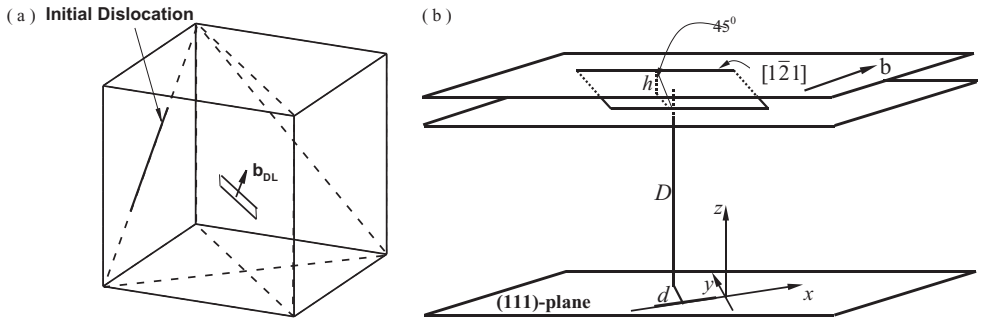

Figure 1. Geometry and initial configuration of a dipolar loop and a glide dislocation. (*a*) Relative positions in three-dimensional geometry. (*b*) Representation of the dipolar loop and dislocation in the local coordinate system.

obtain reliable quantitative data on the sweeping process. For that reason, the parametric dislocation dynamics (PDD) method proposed by Ghoniem *et al* [18, 19] is employed here for the simulation. We study here the influence of forces between small dislocation dipoles on their individual and collective motion in stress gradients. We also investigate the basic mechanism of early clustering and pattering of dipolar loops that is experimentally observed under fatigue loading conditions.

In section 2, we develop a model used to simulate the dynamics of a glide dislocation and interacting dipolar loops. Results of the model are given in section 3, where we investigate the combined motion of a glide dislocation and a single dipolar loop, the behaviour of two dipolar loops with and without their mutual interaction forces, and finally the collective motion of a group of dipolar loops under cyclic applied stress. Finally, conclusions are given in section 4.

2. Dynamics of a glide dislocation and dipolar loops

We analyse here the dynamics of a single glide dislocation and interacting dipolar loops. There are basically four types of dipolar dislocation loops: vacancy and interstitial loops, each in two possible stable configurations [15]. In the analysis here, results for vacancy loops in one of the stable configurations are presented. For interstitial loops and other configurations, the results are similar, and will therefore not be presented.

Figure 1 shows the initial geometry of a glide dislocation and a single dipolar loop. The dislocation can glide on the (111) slip plane, while the dipolar loop can only move along its own glide cylinder, i.e. along the direction of the Burgers vector $[10\bar{1}]$. We assume here that the dipolar loop is a parallelogram. Its two long arms are parallel to the edge orientation $[1\bar{2}1]$ with a length of 60 nm and glide on (111) slip plane, while the two short arms glide on the $(1\bar{1}1)$ slip plane. The relative distance of the two long arms is chosen such that the dipolar loop plane and the glide plane (111) for the two long arms form an angle of 45° as shown in figure 1(*b*). The height of the dipolar loop is taken as 4 nm [20], which is measured by the distance between the two (111) glide planes. The originally straight glide dislocation with the same Burgers vector as the dipolar loop can have any orientation, and is pinned at both ends. We choose the glide plane normal as the z-axis, and the direction of the glide dislocation as the x-axis. The distance between the slip plane of the glide dislocation and the centre of the loop is its stand-off distance, and is denoted by D, as shown in figure 1(*b*). The distance of the projection of the centre of the dipolar loop on the glide plane to the initial dislocation position is denoted by d. Thus, the coordinates of the position of the dipolar loop in this local

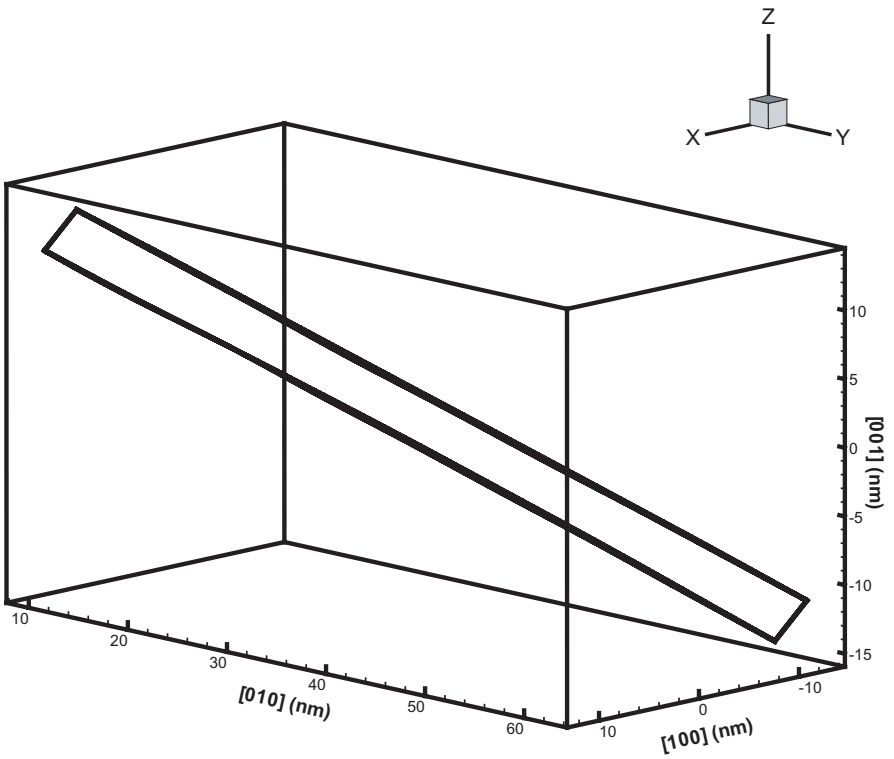

Figure 2. Configuration of the dipolar loop describe in figure 1 under an external shear stress $\tau = 4\,\mathrm{MPa}$, with full interaction between its segments. The coordinates of the dipolar loop centre are (0, 30, 20).

coordinate system can be written as (x, d, D). The geometric configuration and dimensions follow the experimental observations in [20].

Figure 2 shows the deformation of a dipolar loop initially located at $(0, 30, 20)$ under the influence of the glide dislocation and a shear stress $\tau = 4\,\mathrm{MPa}$. The glide dislocation and the four segments of the dipolar loop interact simultaneously under the influence of an external shear stress. It is shown that the deformation of the two short segments is very small, and they are almost straight. The maximum relative deflection of the two long arms is less than 1% of their length. Thus, the overall deformation of the dipolar loop is very small, and can be neglected. As a result, we will assume here that the dipolar loop shape is rigid under relatively low applied shear stresses, and that it moves as a whole along the direction of its Burgers vector. The position of a loop is determined only by the coordinates of its centre. A rigid approximation for the dipolar loop motion is thus possible. In all simulations, the material parameters are for nickel (the shear modulus $\mu = 80\,\mathrm{GPa}$, Poisson's ratio $\nu = 0.33$, and $|\boldsymbol{b}| = 0.25\,\mathrm{nm}$). We also assume that the effect of dislocation dissociation into partials in nickel is small and can be neglected.

The equation of motion for the centre of a loop in the rigid approximation can be written as:

$$\frac{\mathrm{d}x_i^{\mathrm{DL}}}{\mathrm{d}t} = f^{\mathrm{dis}} + \sum_{j \neq i} f_j^{\mathrm{DL}} - f^{\mathrm{friction}} \tag{1}$$

Here, x_i stands for the position of the ith dipolar loop centre along the axis of its glide cylinder. f^{dis} and f_j^{DL} are force components along the glide direction generated by the stress fields of

the glide dislocation and the interaction forces from other dipolar loops, respectively. f^{friction} is the lattice friction, which introduces a threshold for the motion of the dipolar loop [21], it varies with the selection of specific material. The force components f^{dis} and f_j^{DL} have the general form:

$$f = \oint_{\text{DL}} \frac{(\boldsymbol{\sigma} \cdot \boldsymbol{b} \times \boldsymbol{t}) \cdot \boldsymbol{b}}{b} \, \mathrm{d}l \tag{2}$$

where $\boldsymbol{b}$ stands for the Burgers vector, $\boldsymbol{\sigma}$ is the stress field of either the dislocation or of the jth dipolar loop exerted on the ith loop. The stress $\boldsymbol{\sigma}^{\text{dis}}$ is calculated by the fast sum method as introduced in [17]. The stress of a loop $\boldsymbol{\sigma}_j^{\text{DL}}$ is easily computed by summing up the analytical solution [22] of the four straight segments of the dipolar loop. It is to be noted here that a spatially uniform stress field has no effect on the motion of a dipolar loop, as a result of the closed line integration giving a net zero force on the loop.

Once the parametric curve for the dislocation segment is mapped onto the scalar interval $\omega \in [0, 1]$, the stress field everywhere is obtained as a fast numerical quadrature sum [17]. Let us define the following dimensionless parameters: $\boldsymbol{r}^* = \boldsymbol{r}/a, \boldsymbol{f}^* = \boldsymbol{F}/\mu a, t^* = \mu t/B$. Here, a is the lattice constant, μ the shear modulus, B the mobility and t is the time. Following [13], a dislocation can be divided into N_s segments. In each segment Γ_j, we can choose a set of generalized coordinates q_m at the segment ends, thus allowing parametrization of the form: $\boldsymbol{r}^* = \boldsymbol{C}\boldsymbol{Q}$. Here, $\boldsymbol{C} = [C_1(\omega), C_2(\omega), \ldots, C_m(\omega)]$, $C_i(\omega), (i = 1, 2, \ldots, m)$ are shape functions dependent on the parameter $(0 \leqslant \omega \leqslant 1)$, and $\boldsymbol{Q} = [q_1, q_2, \ldots, q_m]^\top$.

Let, $\boldsymbol{f}_j = \int_{\Gamma_j} \boldsymbol{C}^\top \boldsymbol{f}^* |\boldsymbol{ds}|$, $\boldsymbol{k}_j = \int_{\Gamma_j} \boldsymbol{C}^\top \boldsymbol{C} |\boldsymbol{ds}|$ be the total force vector on a curved segment Γ_j, and the corresponding stiffness matrix, respectively. Following a procedure similar to the finite element method (FEM), the equations of motion for all curved segments can be assembled in global matrices and vectors, as:

$$\boldsymbol{F} = \sum_{j=1}^{N_s} \boldsymbol{f}_j, \qquad \boldsymbol{K} = \sum_{j=1}^{N_s} \boldsymbol{k}_j \tag{3}$$

and the equations of motion can be expressed as:

$$\boldsymbol{K} \frac{\mathrm{d}\boldsymbol{Q}}{\mathrm{d}t^*} = \boldsymbol{F} \tag{4}$$

Equation (4) represents a system of ordinary differential equations, which describe the motion of an ensemble of interacting dislocations. Numerical integration of this system of coupled equations (equations (1) and (4)) was carried out by the step forward Euler explicit integration method. The glide dislocation is typically discretized into 22 segments, and cubic splines are used to approximate the shape of each segment. The overall time step is controlled such that the maximum displacement of any dipolar loop or a node on the gliding dislocation is less than 0.01 nm within a time step.

3. Results

Conditions for the dislocation sweeping of dipolar loops proposed by Kratochvíl *et al* [14], as the basic mechanism leading to the formation of PSBs, which was based on the assumptions of the interaction between straight rigid dislocation and dipolar loops, relies on a number of key processes. In this section, we present results that show quantitative assessments of some of the basic ingredients in the sweeping mechanism. First, we analyse the motion of a single dipolar loop that is simultaneously interacting with a glide dislocation. Then, we show results for two dipolar loops interacting with a glide dislocation to quantify the role of inter-dipolar

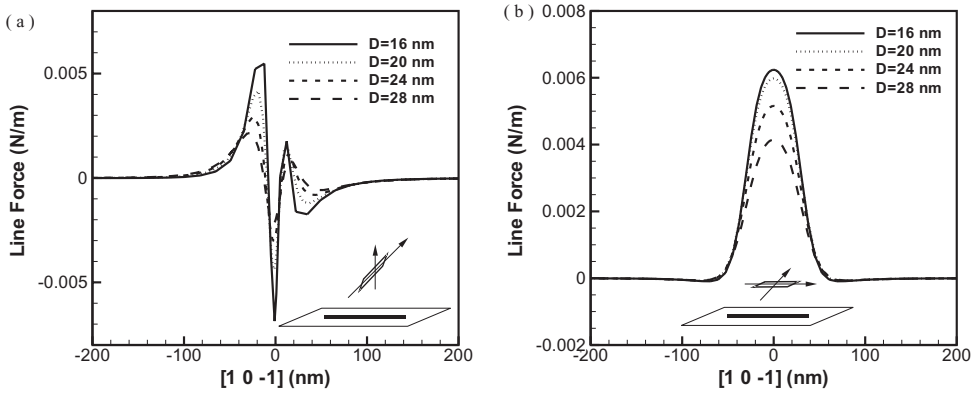

Figure 3. Distribution of line force per unit length generated on an initially straight dislocation line by a dipolar loop situated at various stand-off distances. The coordinates of the dipolar loop are (0, 30, D). (*a*) The direction of the dislocation is normal to the loop's major axis. (*b*) The direction of the dislocation is parallel to loop's major axis.

forces on their coupled motion. And finally, the collective motion of groups of dipolar loops is investigated as a prerequisite for the initiation of PSBs during fatigue loading conditions.

3.1. Glide dislocation and a single dipolar loop

In the following calculations, the position of the dipolar loop relative to the glide plane is (0, 30, D), and the glide dislocation is oriented along $[1\bar{2}1]$. Figure 3(*a*) shows the distribution of the resolved shear force per unit length exerted by the dipolar loop on a straight glide dislocation, which lies along $[10\bar{1}]$, calculated for various stand-off distances. When the main loop axis is normal to the dislocation direction, the dipolar loop generates rapid asymmetric forces on the dislocation, as can be seen in figure 3(*a*). The force distribution on the dislocation is shown in figure 3(*b*), where the main axis of the dipolar loop is oriented along the dislocation line. The force distribution is symmetric in this configuration. The calculations clearly indicate that the range of the dipolar force on the dislocation is fairly localized, and is confined to about twice the larger dimension of the loop (i.e. $\sim$120 nm). As a result of such rapid dipolar force spatial variations, the method of PDD [13] is found to be very suitable.

Dipolar loop forces deform the dislocation line, and this in turn, produces stress gradients in the vicinity of the loop itself. Thus, the mere presence of a dipolar loop close to a straight dislocation generates forces on the loop tending to move it along. Once the effective total force on the dipolar loop exceeds the lattice friction force (the friction stress is assumed to be 8 MPa [21]), the loop moves along its glide cylinder, as governed by equation (1), and consequently changes the force distribution on the dislocation again. Figure 4 shows the simultaneous motion of a dipolar loop and the dislocation as obtained from the numerical integration of equations (1) and (4). The projection of the configuration on the slip plane is shown in figure 4(*a*), while the position of the dipole centre along its glide cylinder is given in figure 4(*b*).

The dipolar loop is swept away from its original location by the stress gradient generated from the curved dislocation. At the beginning of the process, the stress gradient is low, thus the velocity of the dipolar loop is low. After about 0.5 ns, the dipolar loop forces result in higher dislocation curvature. Thus, the loop is driven away faster with an increasing velocity.

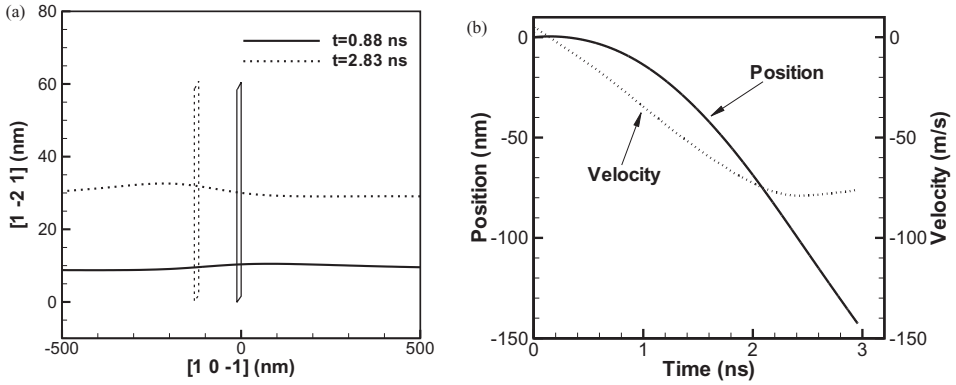

Figure 4. Interaction between a screw dislocation and a mobile dipolar loop under an external shear stress $\tau = 4$ MPa. The initial condition of the dipolar loop is the same as that in figure 3. Note that the scale on the axes is different. (*a*) Relative position of the dipolar loop and configuration of the dislocation at 0.88 ns and 2.83 ns, respectively. (*b*) Loop position and velocity as functions of time.

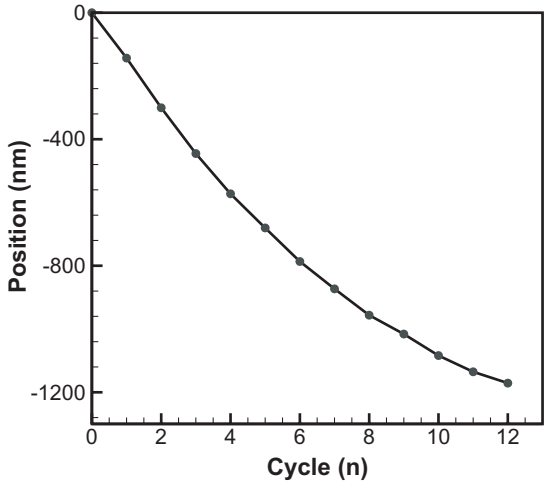

Figure 5. Change of position of the dipolar loop as a function of the number of stress cycles.

At about 2.5 ns, the loop reaches a terminal velocity of about 75 m s^{-1}, as shown in figure 4(*b*). During the simulation, the two ends of the dislocation are pinned. In order to remove boundary effects of the glide dislocation, we choose a long dislocation with an initial length of 4 μm.

Under cyclic stress conditions, the applied stress is reversed within each cycle. We use here an applied shear stress with an amplitude of 4 MPa above the friction stress. The glide dislocation passes back and forth under the dipolar loop. However, the gradient vector of the stress field does not change its sign during stress reversals, because it depends only on the dislocation shape. Thus, the interaction force between the dipolar loop and the dislocation keeps the loop moving along the same initial direction with each oscillation. Figure 5 shows the position of the dipolar loop centre as a function of the number of stress cycles.

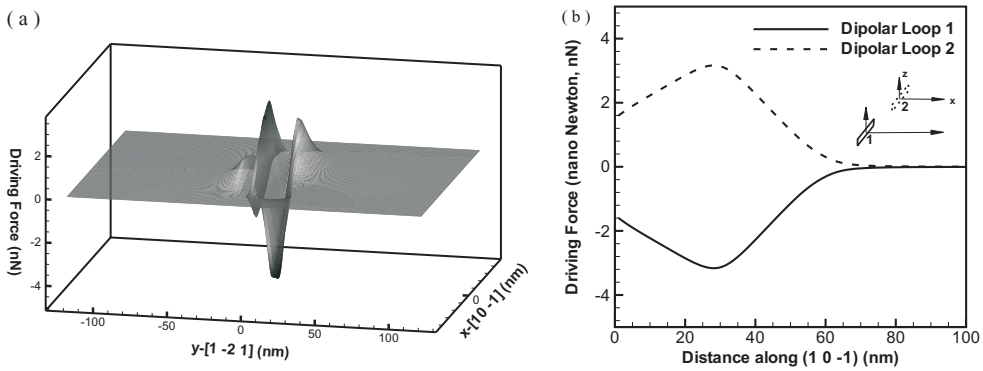

Figure 6. The effect of mutual interaction between two parallel dipolar loops. The stand-off distances are 12 nm and 20 nm, respectively. Both loops have the same Burgers vector $\boldsymbol{b} = [10\bar{1}]$. (*a*) Driving force generated by the first dipolar loop on the second. x and y stand for their relative horizontal distance. (*b*) The same driving force for $y = 0$. The dashed and solid lines stand for the forces of dipolar loops 1 and 2, respectively.

3.2. The effects of mutual interaction between dipolar loops

One important factor that controls the collective motion of dipolar loop groups is the influence of inter-loop forces. To study this effect, we examine here the interaction between two vacancy-type dipolar loops. The force as a function of the mutual position of the two loops is shown in figure 6. The stand-off distances of the loops are 12 nm and 20 nm, respectively. It is shown in figure 6(*a*) that the inter-loop force is a complex function of their relative distance, and that the range of influence is rather small. This feature enables the introduction of a cut-off distance when we perform large-scale simulations. Figure 6(*b*) shows the mutual driving force when the relative $\Delta y = 0$ between loops (refer to figure 1 for the coordinate system). Inter-dipole forces become small and negligible when the relative distance is larger than approximately twice the loop size.

Figure 7 demonstrates the interaction between a glide dislocation and two dipolar loops, initially located at $(-5, 30, 24)$ and $(5, 30, 24)$ respectively. The Burgers vector of the glide dislocation and the loops is $\boldsymbol{b} = \frac{1}{2}[10\bar{1}]$. The dislocation sweeps both loops away to the negative side, as shown in figure 7(*b*). Due to their close distance, the mutual interaction between the two dipoles is very strong. Thus, the second dipolar loop is pushed to the opposite direction until their relative distance is around 40 nm, where their mutual interaction decreases to around zero, They were then moved almost independently by the dislocation cusp, as shown in figure 7(*a*). The stress state of the dipolar loops generated a cusp on the dislocation line. This cusp changes the stress state, and in this way modifies the motion of the dipolar loops.

The importance of inter-loop forces on the dynamics of dipole–dipole–dislocation interactions is demonstrated in figure 8. The centres of two loops are initially located at $(-10, 30, 24)$ and $(10, 20, 24)$. In this configuration, the loops are bound together due to their mutual interaction. If mutual loop interaction is artificially switched off, the two dipolar loops move quite independently from one another, with the latter one moving a little bit faster than the leading one, as seen in figure 8. On the other hand, if mutual interaction is included, inter-loop binding forces are stronger than forces exerted by the glide dislocation. The loops move as a group, with their relative separation almost kept unchanged.

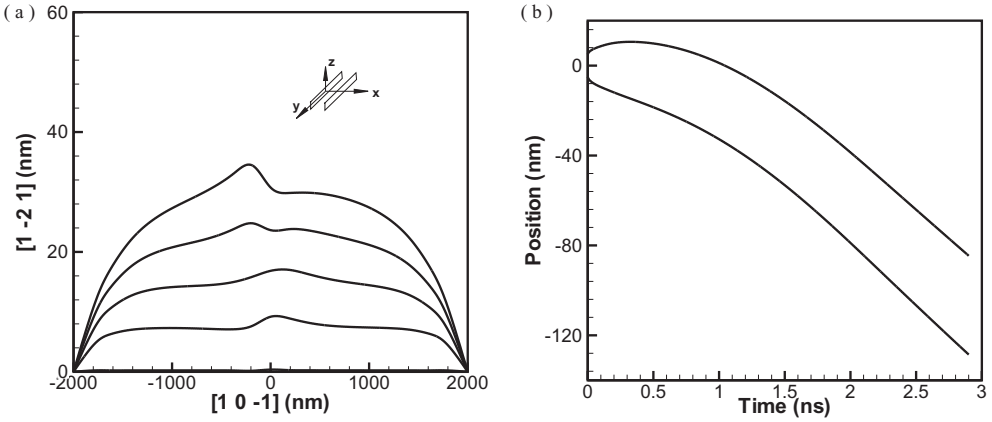

Figure 7. Interaction between a Frank–Read source with an initial screw orientation and two mutually interactive dipolar loops, initially located at $(-5, 30, 24)$ and $(5, 30, 24)$, respectively. Both dislocation and dipolar loops have $\boldsymbol{b} = \frac{1}{2}[10\bar{1}]$. (*a*) Dislocation configuration at different times (time interval $\Delta t = 0.7$ ns). (*b*) Change of position for the two loops as a function of time.

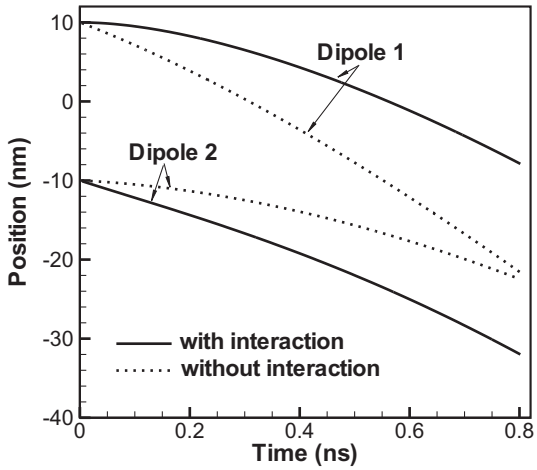

Figure 8. Comparison between the effects of including and excluding the mutual interaction of the two dipolar loops. The two dipolar loops are initially located at $(-10, 30, 24)$ and $(10, 20, 24)$, respectively.

3.3. Collective motion of dipolar loops

To demonstrate the collective sweeping of dipolar dislocation loops, the dynamics of interaction between a glide dislocation and 20 loops is simulated. The dislocation is pinned at its ends, representing a Frank–Read source, and is cycled by the applied stress. The loops are initially randomly distributed in the vicinity of the dislocation slip plane, in the range of distances -300 nm to 300 nm, as shown in figure 9(*a*). The dislocation line is very long ($4\,\mu$m), so as to remove the effects of pinning boundary conditions on dipolar loop dynamics. Successive configurations of this system are shown in figures 9(*b*)–(*d*). After a critical number of cycles, dipolar loops separate into two clusters, and both groups move in the negative direction. The dynamics of the interaction process is displayed in a *trajectory* plot, shown in figure 10. Two

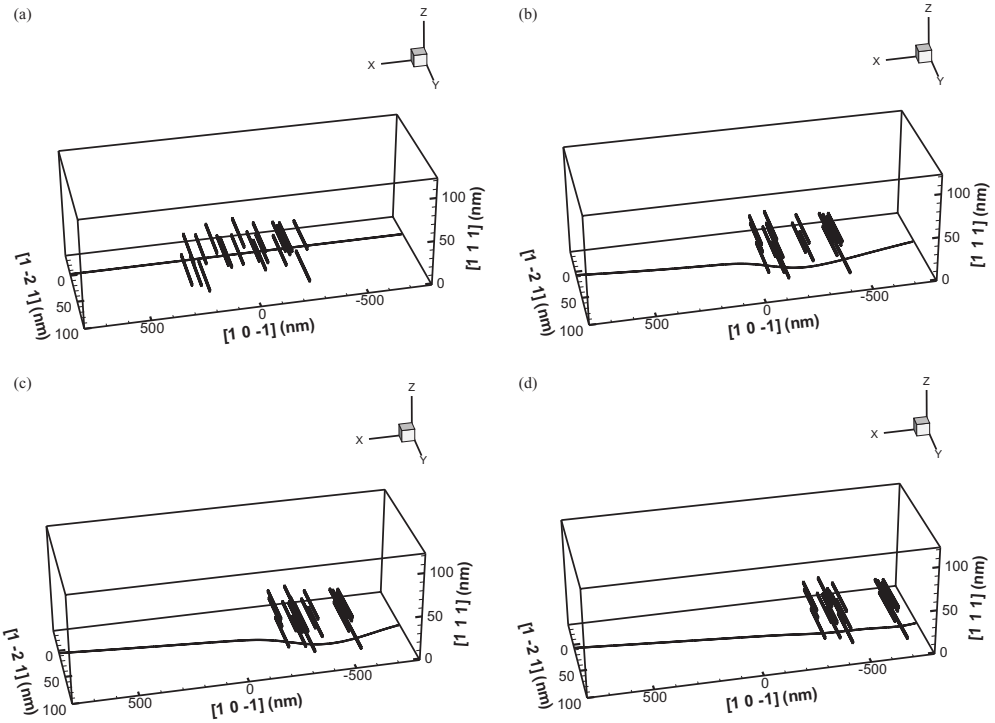

Figure 9. The relative configuration of 20 dipolar loops at the end of different cycles: (*a*) initial, (*b*) 5th cycle, (*c*) 10th cycle, (*d*) 15th cycle.

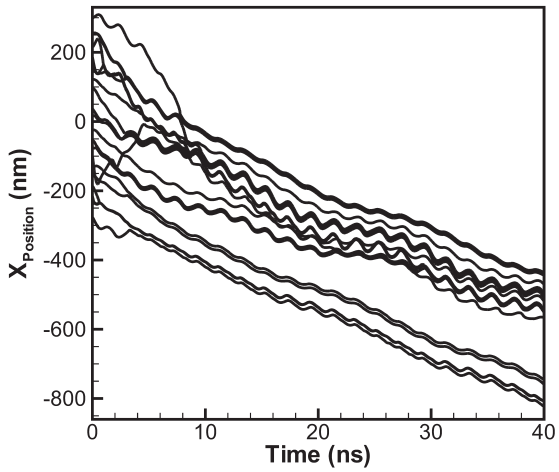

Figure 10. *Trajectory* plot of the dynamics of 20 interacting dipolar loops, driven by an oscillating screw dislocation.

well-separated loop clusters are formed after a number of cycles of the order of 20, as can be seen in figures 9(*d*) and 10. Some loop pairs are strongly coupled together, retaining their relative positions throughout the entire simulation (see the trajectories of two loops at the lower end of figure 10), while most others execute complex trajectories that cannot be predicted

a priori. Nevertheless, the final configuration is represented by dipolar loop clusters swept into two well-separated groups. The glide dislocation then moves in the loop-free channel.

4. Conclusions

The results presented here show that the PDD method [17, 18] is a convenient tool for studies of elementary mechanisms of dislocation pattering caused by elastic interactions amongst defects. The method is accurate enough to deal with complex stress fields associated with the dynamic motion of dipolar dislocation loops and glide dislocations. The present investigation has demonstrated a number of physical processes involved in the sweeping mechanism:

(i) The stress field of a dipolar loop forms a small cusp on the glide dislocation, which localizes high stress gradients in its vicinity, and the loop appears to be riding on that cusp.

(ii) Detailed investigation of loop–loop interaction forces show that such forces are critically important to the sweeping mechanism. The cusp on the dislocation line caused by one loop leads to indirect coupling with other loops, and this effect facilities loop cluster formation. On the other hand, when two loops are on different glide cylinders, and their inter-loop force barrier is overcome by the force exerted by the glide dislocation, loops trap one another in their mutual interaction field and move together. This self-trapping effect appears to be essential to the formation of loop clusters.

(iii) Dislocation dynamics simulations demonstrate that the loop clustering mechanism plays an important role in the process of sweeping, which results from the complex interaction between loops and glide dislocations. The sweeping process has been tested using fixed-ends of a glide dislocation that is about 4 μm long and 20 rigid dipolar loops.

Acknowledgments

Research is supported by the US Department of Energy, Office of Fusion Energy, through Grant DE-FG02-03ER54719, by the National Science Foundation through grant NSF-DMR-0113555 with UCLA, and by the Grant Agency of the Czech Republic, through Grant 106/00/1109.

References

[1] Kratochvíl J and Saxlova M 1992 *Scr. Metall. Mater.* **26** 113–16
[2] Kratochvíl J and Saxlova M 1993 *Phys. Scr.* **49** 399–404
[3] Malygin G A 1995 *Solid State Phys.* **37** 3–42
[4] Glazov M, Llanes L M and Laird C 1995 *Phys. Status Solidi* (a) **149** 297–321
[5] Glazov M and Laird C 1995 *Acta Metall. Mater.* **43** 2849–57
[6] Saxlova M, Kratochvíl J and Zatloukal J 1997 *Mater. Sci. Eng.* A234–6
Saxlova M, Kratochvíl J and Zatloukal J 1997 *Mater. Sci. Eng.* 205–8
[7] Malygin G A 1999 *Prog. Phys.* **169** 979–1010
[8] Kratochvíl J 2001 *Mater. Sci. Eng.* A **309–310** 331–5
[9] Ghoniem N M and Amodeo R J 1990 (Netherlands: Kluwer) p 303
[10] Devincre B and Kubin L 1994 *The Japan Institute of Metals* pp 179–89
[11] Fournet R and Salazar J M 1996 *Phys. Rev.* **53** 6283–90
[12] Devincre B 1996 (Netherlands: Kluwer) pp 309–23
[13] Ghoniem N M, Tong S-H and Sun L Z 2000 *Phys. Rev.* B **61** 913
[14] Kratochvíl J, Kroupa F and Kubin L P 1999 *Proc. 20th Riso International Symp. on Materials Science: Deformation-Induced Microstructures: Analysis and Relation to Properties (Riso National Laboratory, Roskilde, Denmark)* ed J B Blide-Sorensen *et al*, pp 387–92

[15] Verecký S, Kratochvíl J and Kroupa F 2002 *Phys. Status Solidi* a **191** 418–26
[16] Khraishi T A and Zbib H M 2002 *Phil. Mag. Lett.* **82** 265–77
[17] Ghoniem N M and Sun L Z 1999 *Phys. Rev.* B **60** 1
[18] Ghoniem N M, Huang J and Wang Z 2002 *Phil. Mag. Lett.* **82** 55–63
[19] Jianming H and Ghoniem N M 2003 *Modell. Simul. Mater. Sci. Eng.* **11** 21–39
[20] Tippelt B, Bretschneider and Hahner P 1997 *Phys. Stat. Sol.* (a) **163** 11–26
[21] Kubin L P and Kratochvíl J 2000 *Phil. Mag.* A **80** 201–18
[22] Devincre B 1995 *Solid State Commun.* **93** 875–8

Summary of Comments on msms180705

Page: 11

Sequence number: 1
Author:
Date: 5/29/2004 2:24:02 PM
Type: Highlight
[9]

Sequence number: 2
Author:
Date: 5/29/2004 2:27:48 PM
Type: Note
Au: Could you please provide the title of the book for reference [9]

Sequence number: 3
Author:
Date: 5/29/2004 2:25:11 PM
Type: Highlight
[10]

Sequence number: 4
Author:
Date: 5/29/2004 2:25:16 PM
Type: Highlight
[12]

Sequence number: 5
Author:
Date: 5/29/2004 2:32:06 PM
Type: Note
Au: Could you please provide the book titles for reference [10] and [12]

Page: 12

Sequence number: 1
Author:
Date: 5/29/2004 2:30:53 PM
Type: Highlight
Bretschneider

Sequence number: 2
Author:
Date: 5/29/2004 2:31:02 PM
Type: Note
Au: Could you please provide initials